

**LA-UR-23-21983**

Accepted Manuscript

# Modeling the Effect of Surface Platinum-Tin Alloys on Propane Dehydrogenation on Platinum-Tin Catalysts

Fricke, Charles Henry  
Bamidele, Olajide H.  
Bello, Mubarak  
Chowdhury, Jawad  
Terejanu, Gabriel  
Heyden, Andreas

Provided by the author(s) and the Los Alamos National Laboratory (2023-08-14).

**To be published in:** ACS Catalysis

**DOI to publisher's version:** 10.1021/acscatal.3c00939

**Permalink to record:**

<https://permalink.lanl.gov/object/view?what=info:lanl-repo/lareport/LA-UR-23-21983>



Los Alamos National Laboratory, an affirmative action/equal opportunity employer, is operated by Triad National Security, LLC for the National Nuclear Security Administration of U.S. Department of Energy under contract 89233218CNA000001. By approving this article, the publisher recognizes that the U.S. Government retains nonexclusive, royalty-free license to publish or reproduce the published form of this contribution, or to allow others to do so, for U.S. Government purposes. Los Alamos National Laboratory requests that the publisher identify this article as work performed under the auspices of the U.S. Department of Energy. Los Alamos National Laboratory strongly supports academic freedom and a researcher's right to publish; as an institution, however, the Laboratory does not endorse the viewpoint of a publication or guarantee its technical correctness.

**Modeling the Effect of Surface Platinum-Tin Alloys on Propane  
Dehydrogenation on Platinum-Tin Catalysts**

Charles H. Fricke<sup>1</sup>, Olajide H. Bamidele<sup>1</sup>, Mubarak Bello<sup>1</sup>, Jawad Chowdhury<sup>2</sup>, Gabriel  
Terejanu<sup>2\*</sup>, Andreas Heyden<sup>1\*</sup>

<sup>1</sup>*Department of Chemical Engineering, University of South Carolina, Columbia, South Carolina,  
29208, USA*

<sup>2</sup>*Department of Computer Science, University of North Carolina at Charlotte, Charlotte, North  
Carolina, 28223, USA*

**Authors to Address Correspondence:** heyden@cec.sc.edu; gterejan@uncc.edu

## Abstract

Uncertainty analysis, reported experimental literature data, and density functional theory were synthesized to model the effect of surface tin coverage on platinum-based catalysts for non-oxidative propane dehydrogenation to propylene. This study tests four different platinum-tin skin surface models as potential catalytic sites, these being Pt<sub>3</sub>Sn/Pt(100), PtSn/Pt(100), Pt<sub>3</sub>Sn/Pt(111), and Pt<sub>2</sub>Sn/Pt(211), and compares them to the corresponding pure Pt surface sites using an uncertainty analysis methodology that uses BEEF-vdW with its ensembles (BMwE) to generate the uncertainty for the energies of the intermediates and transition states. One experimental data set with two experimental observations, selectivity to propylene and turnover frequency of propylene, was used as a calibration data set to evaluate the impact of the experimental data on informing the models. This study finds that the prior model for Pt<sub>3</sub>Sn/Pt(100) is the most active and Pt<sub>2</sub>Sn/Pt(211) is most selective towards propylene. Active sites on the (100) facet have the highest probability of being responsible for C<sub>1</sub> and C<sub>2</sub> product formation (C-C bond cleavage). Increasing the Sn coverage on the (100) surface facet to a PtSn/Pt(100) active site leads to a significantly reduced rate and might explain the experimentally observed higher selectivity of Sn doped catalysts relative to pure Pt catalysts. Next, this study finds that for all surfaces, except PtSn/Pt(100), the rate-controlling steps are the first initial dehydrogenation steps alongside some partially rate controlling second dehydrogenation steps. For PtSn/Pt(100), only the first dehydrogenation step to CH<sub>3</sub>CH<sub>2</sub>CH<sub>2</sub>\* and second dehydrogenation steps are rate controlling. Next, the calibrated models for all surfaces were found to be selective towards propylene production and model the reported turnover frequency successfully. Nevertheless, Pt<sub>2</sub>Sn/Pt(211) emerges as the active site with some (minor) evidence as main active site based on Jeffreys' scale interpretation of Bayes

factors. This observation agrees with prior studies that also find step sites to be most likely the most relevant active sites for pure Pt catalysts. Overall, the results indicate that tin, in addition to affecting the binding strength of the adsorbed species, prevents deeper dehydrogenation (reducing coking) and cracking reactions through increasing activation barriers for unwanted side reactions.

## Introduction

Propylene production from propane is an industrially important reaction, due to the usage of propylene as a chemical feedstock, and the changing economics of propane to propylene dehydrogenation.<sup>1</sup> Non-oxidative propane dehydrogenation (PDH) on platinum-tin catalysts continues to be a significant industrial process of producing propylene, due to its high selectivity to propylene.<sup>2,3</sup> Many experimental studies have been done to evaluate the effect of alloying platinum with tin on propane dehydrogenation.<sup>4-22</sup>

For example, in Barias et al., Pt and Pt-Sn alloy nanoparticles were evaluated for propane dehydrogenation.<sup>6</sup> It was found that the single metal platinum nanoparticles were less selective than the alloyed nanoparticles, with the pure metal particles having a selectivity toward propylene of 85% while the Pt-Sn particles had a selectivity close to 97%. In addition, it was found that the turnover frequencies for propylene production were close to three times higher on Pt-Sn catalysts than on Pt catalysts, and that carbon deposition on the Pt-Sn catalysts was much less than on the Pt catalysts. Similar results were found by Kaylor and Davis,<sup>7</sup> where on silica supported catalysts, Pt-Sn exhibited a much higher selectivity to propylene than on platinum-only catalysts.

In Wang et al., work was performed to analyze the regeneration of Pt-Sn alloy catalyst particles, by measuring the depletion of tin and the following regeneration of the Pt-Sn surface by segregation processes that occur in the Pt-Sn alloy particle.<sup>4</sup> They find that the particles, after undergoing etching of the original tin and then a regeneration treatment to drive tin from the bulk of the particle to the surface, maintain a selectivity of 92% to propylene, with minimal effects on

the catalytic properties of the particles. Similar results with Sn enriched surfaces for Pt-Sn catalysts for propane dehydrogenation were seen by Zhua et al.<sup>5</sup>

In addition to the experimental literature, many density functional theory-based studies have been performed to analyze the impact of tin on platinum-tin catalysts for alkane dehydrogenation.<sup>23-28</sup> One such study by Nam and Celik was performed to analyze the differences between three surfaces Pt(111), Pt<sub>3</sub>Sn(111), and a Pt<sub>3</sub>Sn surface skin alloy on a bulk Pt(111) surface for ethane dehydrogenation.<sup>23</sup> They found that increasing Sn in the surface skin alloy may increase the selectivity, while forming a bulk alloy may not increase selectivity as significantly, as they find that the surface skin alloy has a higher selectivity to propylene relative to the bulk alloy. This surface skin alloy behavior may better replicate what is seen experimentally by Wang et al. and Zhua et al.<sup>4,5</sup> Specifically, Wang et al. report, based on TEM and EDS data, that the Pt-Sn surface alloy remains stable after the propane dehydrogenation reaction.<sup>4</sup> However, disagreements do arise, as Yang et al. finds that the bulk Pt<sub>3</sub>Sn alloy for Pt(111) may be the most active of the alloys.<sup>24</sup> The majority of density functional theory studies research Pt(111) and Pt(211) facets, in which they model either the facet to be composed of a bulk alloy, or the pure platinum facet with a surface Pt-Sn alloy skin.<sup>25,26</sup> Pt-Sn alloys cleaved in the (100) direction are not well studied, though it was found by Fricke et al. that Pt(100) has high turnover frequencies for propane consumption and possibly a low selectivity to propylene.<sup>29</sup>

In this work, we seek to identify how Sn doping modifies the kinetics of the surface facets of Pt particles for the non-oxidative dehydrogenation of propane to propylene. Specifically, we studied four model surfaces, Pt<sub>3</sub>Sn/Pt(100), PtSn/Pt(100), Pt<sub>3</sub>Sn/Pt(111), and Pt<sub>2</sub>Sn/Pt(211) using density functional theory (DFT) calculations, uncertainty analysis using the BEEF-vdW with its ensembles (BMwE) model and published experimental literature data. Given

the diversity in Sn distributions in a Pt-Sn alloy, we limit this study to surface skin alloys on a Pt core. Likely, such models are most meaningful for small concentrations of Sn given that Sn tends to segregate to the surface.<sup>4</sup> While modeling each facet, kinetic data such as turnover frequencies (TOF) for propylene production and other product gases, apparent activation energies, reaction orders, and selectivities to different product gases are reported. Finally, this study also identifies the mechanism and rate-controlling species for these alloys and compares the activity and selectivity of Pt-Sn alloy catalysts to pure platinum catalysts.

## Methods

### Computational Details

Calculations were performed using the Vienna Ab initio Simulation Program (VASP) version 5.4.4.<sup>30-32</sup> BEEF-vdW was the functional chosen for this study.<sup>33</sup> In previous work, it was found that BEEF-vdW with its ensembles (BMwE) was more successful in describing platinum surface behavior than an alternative method based on multiple DFT functionals to describe the uncertainty in the functional choice.<sup>29</sup> A Methfessel-Paxton order of 1 with an electron smearing width of 0.2 eV was used to model the electronic occupancies.<sup>34,35</sup> In addition, an energy cutoff of 400 eV with a  $5 \times 5 \times 1$  reciprocal grid using Monkhorst-Pack was found to be well converged for the calculations.<sup>36,37</sup> The energy convergence criterion was  $1 \times 10^{-7}$  eV, and the force convergence criterion was 0.03 eV/Å. To correct for errors in the entropy calculation within the harmonic approximation for small frequencies, frequencies less than  $50 \text{ cm}^{-1}$  were corrected to  $50 \text{ cm}^{-1}$ .<sup>38</sup> Transition states were first converged with nudged elastic band calculations, and then with dimer calculations using VTST to ensure that the transition states were well optimized.<sup>39-42</sup> In addition, for each transition state, a frequency calculation was performed to verify that there

was only one imaginary frequency and that it corresponded to the desired bond cleavage. 46 intermediate species and 130 transition states were optimized for each surface model. Part of the reaction network is pictorially described in Figure 1. All elementary reactions considered are tabulated in the Supporting Information Table S1-S6.

Four surfaces were tested in this study, Pt<sub>3</sub>Sn/Pt(100), PtSn/Pt(100), Pt<sub>3</sub>Sn/Pt(111), and Pt<sub>2</sub>Sn/Pt(211). They were chosen to evaluate how a substitutional replacement of platinum with tin would affect the bonding strength of intermediates and transition states. Figure 2 illustrates the four surface-skin models that were chosen based on a potential geometric effect of tin on the Pt surface. For example, Pt<sub>3</sub>Sn/Pt(100) replaces one of the platinum atoms present in each of the four-fold hollow sites with a tin atom, while PtSn/Pt(100) replaces two of the platinum atoms present in the four-fold hollow site with tin atoms and all of the bridge sites contain a tin atom. Pt<sub>3</sub>Sn/Pt(111) models the effect of tin on some of the fcc and hcp sites such that larger surface-adsorbed species have to interact with Sn. The Pt<sub>2</sub>Sn/Pt(211) model was chosen as it modeled both the effect of the substitution of tin for platinum on the four-fold hollow site and the fcc and hcp sites present near the edge. While many more different Pt-Sn arrangements are theoretically possible, we expect these models allow us to qualitatively understand the effects of Sn alloying on the activity and selectivity of the underlying Pt catalyst.

The Pt<sub>3</sub>Sn/Pt(100), PtSn/Pt(100), and Pt<sub>3</sub>Sn/Pt(111) surfaces were modeled as 4×4×4 layer, 64 atom slabs, with a 15 Å vacuum gap added to prevent periodic interactions. The Pt<sub>2</sub>Sn/Pt(211) model is a 6 layer, 80 atom slab, with a 15 Å vacuum gap added to prevent periodic interactions. All alloys are energetically favored to form, with energies of formation of -0.640 eV or greater, with the exception of PtSn/Pt(100), which has a formation energy of +0.01 eV. We note that while the PtSn/Pt(100) surface is only marginally stable, it was specifically

chosen here since Pt(100) was previously found to be the most unselective Pt surface for propane dehydrogenation and at a stoichiometric surface Sn coverage all bridge sites must involve both Sn and Pt, i.e., a large surface Sn coverage has the potential to significantly change the activity and selectivity of the (100) facet. The formation energies of all alloys are summarized in Section 8 of the Supporting Information (see Table S22). Figure 2 illustrates all surfaces. Surface slab parameters and coordinates of all surface intermediates and transition states can be found in the Supporting Information as additional text files.

As mentioned in the previous section, BEEF-vdW with its ensembles (BMwE) was chosen to represent the uncertainty within the functional energy for the models.<sup>29,43</sup> Previous work found that this was a more supported model for describing platinum surface behavior when used for calibrating on experiments. The methodology for generating this model is the same as in Fricke et al., save that BEEF-vdW was used to optimize the entire system, instead of just as a single-point energy calculation.<sup>29</sup> This involves using the 2000 BEEF-vdW ensemble energies for each structure together with the optimized mean energies to perform a factor analysis, and from that generating the covariance matrix to create the uncertainty and uncertainty correlation around each species energy. We believe that the differences between the optimized versus single point energies are small in comparison to the total uncertainty in the functional errors, and this allows for data comparison between this study and our prior platinum-only study. From the prior platinum-only study, some of the intermediates and transition states structures were re-optimized, and better local minima were obtained. All optimized structures including recently updated ones can be found in the Supporting Information.

A common challenge present in computational heterogeneous catalysis is that few experimental data sets have been published on the reaction systems of interest that can be

calibrated on, and as such, comparisons will be made between the prior model, without calibration, and the posterior model, with calibration. Specifically, the experiment from Barias et al. is calibrated against, which was performed at 792 K and at approximately 0.29 bar of propane and 0.1 bar H<sub>2</sub>.<sup>6</sup> The data is calibrated on the turnover frequency of propane and selectivity to propylene. Selectivity to propylene is defined as:

$$Selectivity = \frac{TOF_{Propylene}}{TOF_{Propane}} \quad (1)$$

where  $TOF_{Propylene}$  is the turnover frequency of propylene, and  $TOF_{Propane}$  is the turnover frequency of propane, defined as number of propylene molecules produced per second per site and number of propane molecules consumed per second per site, respectively.

Given the experimental data,  $D = [TOF_{propylene}, Selectivity]$ , the likelihood function  $p(D|\theta, M)$  assumes independence between experimental measurements and it is defined similarly to our previous work.<sup>29,44,45</sup>

$$p(D|\theta, M) = p(TOF_{propylene}|\theta, M) * p(Selectivity|\theta, M) \quad (2)$$

A transformation was applied to the selectivity data using a logit function, as selectivity must be within the bounds of [0,1]. This transformation was done to change the function range to  $(-\infty, \infty)$  which is necessary to properly include and analyze the errors. The logit function for selectivity is defined as the following.<sup>46</sup>

$$logit(Selectivity) = \ln\left(\frac{Selectivity}{1 - Selectivity}\right) \quad (3)$$

In addition, a similar rationale was determined for transforming the  $TOF_{Propylene}$  data into the  $\log_{10}TOF$  data to evaluate the errors present in the model on the range from  $(-\infty, \infty)$ .

Combining the above equations, we find that the full description of the likelihood function is:

$$p(D|\theta, M) = \frac{1}{\sqrt{2\pi\sigma_{TOF}^2}} \exp\left(-\frac{1}{2} \frac{(\log_{10}TOF - \log_{10}TOF^*)^2}{\sigma_{TOF}^2}\right) * \frac{1}{\sqrt{2\pi\sigma_{logit(Selectivity)}^2}} \exp\left(-\frac{1}{2} \frac{(\logit(Selectivity) - \logit(Selectivity)^*)^2}{\sigma_{logit(Selectivity)}^2}\right) \quad (4)$$

where  $\sigma_{TOF}^2$  is the variance of the turnover frequency of propylene,  $\sigma_{logit(Selectivity)}^2$  is the variance of the selectivity to propylene,  $\log_{10}TOF^*$  and  $\logit(Selectivity)^*$  are the model values of propylene turnover frequency and selectivity, and  $\log_{10}TOF$  and  $\logit(Selectivity)$  are the reported experimental values of the TOF and selectivity. Details for the distributions of the variances can be found in Section 3 and Table S7 of the Supporting Information.

The Quantification of Uncertainty for Estimation, Simulation, and Optimization (QUESO) package was used to perform the statistical forward problem and calibration problem.<sup>47</sup> The multilevel Monte Carlo implementation in QUESO was used to calibrate the microkinetic model using experimental data.<sup>48,49</sup>

### 3.2.2 Microkinetic Modeling

To calculate the adsorption free energies, the free energy of the gas phase species and the clean surface slab are subtracted from the free energy of the adsorbed species.

$$\Delta G_{ads,i} = G_{slab,i} - G_{slab} - G_{i,gas} \quad (5)$$

where  $\Delta G_{ads,i}$  is the free energy of adsorption of intermediate i,  $G_{slab,i}$  is the free energy of the slab with adsorbed intermediate i,  $G_{slab}$  is the free energy of the clean slab,  $G_{i,gas}$  is the free energy of the gas phase species.

The activation free energy is defined as the following and the forward rate constants are computed using harmonic transition state theory (hTST).

$$\Delta G_j^\ddagger = G_j^\ddagger - \sum G_{ads,j}^R \quad (6)$$

$$k_{for,j} = \frac{k_B T}{h} e^{-\frac{\Delta G_j^\ddagger}{k_B T}} \quad (7)$$

where  $\Delta G_j^\ddagger$  is the activation free energy of reaction j,  $G_{j,i}^\ddagger$  is the free energy of the transition state in reaction j,  $G_{ads,j}^R$  is the reactant free energy of adsorption for reaction j, and  $k_{for,j}$  is the forward rate constant.

Collision theory was used for calculating adsorption rate constants using the following equation:

$$k_{ads} = \frac{1}{N_0 \sqrt{2\pi m_A k_B T}} \quad (8)$$

where  $N_0$  is the number of sites per surface area, and  $m_A$  is the molecular weight of species A.

For calculating the entropic contributions to the Gibbs free energy, the harmonic approximation was used. There are many questions about the accuracy of the harmonic approximation for calculating the entropies of the adsorbed molecules.<sup>50-52</sup> While including the uncertainty from the entropy calculations into our models is desirable, this was not done here

given the difficulty in estimating the correlation of the entropy uncertainty for the various surface species. Previous work found that the 95% confidence interval around many species based on the functional uncertainty is approximately 0.7 eV; thus, the functional uncertainty is likely much larger than the effect of the entropic uncertainty on the Gibbs free energy for small molecules, justifying our procedure.<sup>29</sup> Nevertheless, in future work we plan on developing procedures for properly considering the entropy uncertainty on microkinetic models.

In all of the Pt-Sn surface model simulations, the free sites made up more than 90% of the total sites present on each surface, and so lateral interactions of surface species were not considered. However, at the reaction condition, significant surface coverage of hydrocarbon species was found for the pure platinum surface models. CH species was found on Pt(111) and CHCH species on Pt(100) surface, while free sites are predominant on the Pt(211) surface. A linear lateral interaction model was therefore used to account for the effect of surface species on adsorption energies and transition state barriers. Lateral interaction methods and parameters for Pt(100) and Pt(111) models are further described in Section 4 of the Supporting Information (see Figures S1 and S2 and Table S11). Section 4 of the Supporting Information also contains a description of the number of sites occupied by each species on each surface model (Table S9 and S10).

Reaction orders in H<sub>2</sub> and CH<sub>3</sub>CH<sub>2</sub>CH<sub>3</sub> were calculated using the following equation:

$$\alpha_i = \left( \frac{\partial \ln(TOF)}{\partial \ln(P_i)} \right)_{T, P_{j, j \neq i}} \quad (9)$$

where  $\alpha_i$  is the reaction order of species *i*, ln(TOF) is the natural logarithm of the turnover frequency of propylene, and ln( $P_i$ ) is the natural logarithm of the partial pressure of species *i*.

We also calculated the apparent activation energy, using the following equation:

$$E_{app} = -k_B \left( \frac{\partial \ln(TOF)}{\partial \left(\frac{1}{T}\right)} \right)_{P_i} \quad (10)$$

where  $E_{app}$  is the apparent activation energy.

Degrees of kinetic rate control using Campbell's degree of rate control theory were calculated using the following equation:

$$X_{KRC,i} = \left[ \frac{\partial \ln(TOF)}{\partial \left( \frac{\Delta G_i^\ddagger}{-k_B T} \right)} \right]_{T, P_i, \Delta G_i^{ads}, \Delta G_{j, j \neq i}^\ddagger} \quad (11)$$

where  $X_{KRC,i}$  is the degree of kinetic rate control.<sup>53-55</sup>

The reaction network studied includes coking and deep-dehydrogenation steps. The intermediates and transition states can be found in Section 1 of the Supporting Information.

## Results and Discussion

For each catalyst model, a separate microkinetic model, uncertainty quantification, and gas-phase corrections were created to generate the quantities of interest for each experimental result. Section IX of the Supporting Information (Figure S8 and S9) illustrate the pairwise distributions of  $\log_{10}$ TOF and selectivity and we observe that relatively low and high rates can be found for both low and high selectivities, justifying our statistical approach for analyzing our results. Figure 3 describes the distribution of the turnover frequencies for propylene and selectivity to propylene for each surface. All simulations were ran at 792K, with partial pressures of propane and H<sub>2</sub> at 0.29 bar and 0.09 bar, respectively, to model Barias et al.<sup>6</sup> As shown in this figure and described in Table S21 of the Supporting Information, Pt<sub>2</sub>Sn/Pt(211) is on average the

most selective of the surfaces, followed by PtSn/Pt(100), Pt<sub>3</sub>Sn/Pt(100), and then Pt<sub>3</sub>Sn/Pt(111). It is interesting to note that Pt<sub>3</sub>Sn/Pt(111), despite showing the lowest selectivity to propylene of the four surfaces, has the highest selectivity for propyne. As a result, and as illustrated in Figure S5 and S6 of the Supporting Information, it is the active sites on the (100) surface facet that display the highest selectivity towards non-C<sub>3</sub>, i.e., C<sub>1</sub> and C<sub>2</sub>, products (promote C-C bond cleavage).

In contrast, the turnover frequency of propylene and consumption of propane is on average highest for Pt<sub>3</sub>Sn/Pt(100), then Pt<sub>2</sub>Sn/Pt(211), Pt<sub>3</sub>Sn/Pt(111), and finally PtSn/Pt(100). The selectivity and turnover frequency differences can be viewed as a function of multiple factors. One of these factors is the activation energy of key steps surrounding the propane to propylene reaction. As shown in Table 1, the selectivity is highest when the barriers for further dehydrogenation or cracking of propylene are comparatively high, or activation barriers for alternative dehydrogenation of the C<sub>3</sub>H<sub>7</sub> species are higher than the dehydrogenation of C<sub>3</sub>H<sub>7</sub> to propylene. This is especially evident for Pt<sub>3</sub>Sn/Pt(100), where the reaction barrier for competing products from the C<sub>3</sub>H<sub>7</sub> intermediate are significantly lower than to the dehydrogenation to produce adsorbed propylene. Specifically, Reaction 7, as described in Table 1, which constitutes the full dehydrogenation reaction of the central carbon atom, possesses a lower activation free energy by 0.23 eV than Reaction 3 which is the dehydrogenation of a terminal carbon to produce the desired adsorbed propylene species. For the Pt<sub>3</sub>Sn/Pt(111) model, the alternative second dehydrogenation pathway to non-propylene species is kinetically also favored but only by 0.03 eV which is clearly within the uncertainty of the DFT calculations. In contrast, for Pt<sub>2</sub>Sn/Pt(211) and PtSn/Pt(100), Reaction 3 is kinetically favored over Reaction 7. Similarly, the terminal carbon dehydrogenated propane species can be further dehydrogenated at the terminal carbon

(Reaction 11) or dehydrogenated at the central carbon to produce adsorbed propylene (Reaction 4). For all but the stepped Pt<sub>2</sub>Sn/Pt(211) surface, this alternative dehydrogenation pathway is more kinetically favorable than propylene production, due to the lower activation barrier. Finally, the lower observed selectivity to propylene of Pt<sub>3</sub>Sn/Pt(100) can be further explained by the kinetics of the deep dehydrogenation and cracking of propylene. The free energy of the transition states for Reactions 20, 22, and 23 are all considerably lower for Pt<sub>3</sub>Sn/Pt(100) than for the two higher selectivity surfaces, PtSn/Pt(100) and Pt<sub>2</sub>Sn/Pt(211). Also, Pt<sub>3</sub>Sn/Pt(111) has generally higher transition state free energies for most C-C bond cleavage reactions compared to Pt<sub>3</sub>Sn/Pt(100), explaining the relatively higher selectivity to C<sub>3</sub> products (propylene and propyne), i.e., low selectivity to C<sub>1</sub> and C<sub>2</sub> products (see Figure S5 and S6).

Free energy differences of the various states on the different surfaces can largely be explained by geometric effects that the substitution of tin has on these alloy surfaces. For Pt<sub>3</sub>Sn/Pt(100) and PtSn/Pt(100), most of the intermediates bind less strongly to the alloy surface than to the pure platinum surface, due to most hydrocarbons having to bind to multiple surface atoms and some of them containing Sn. This is most evident for carbon on the surface, which cannot bind to four platinum atoms at the surface due to the substitution of tin on the surface at either 3:1 or 1:1 ratios on these surface alloys on Pt(100). These substitutional effects are most pronounced for PtSn/Pt(100), due to its effects on both the bridge and hollow sites. This explains the severe decrease in turnover frequency seen in Figure 3 for the PtSn/Pt(100) alloy, even though the free site coverages are high, i.e., they are on average 89%, as described in Table S20 in the Supporting Information.

Next, a combination of geometric and electronic factors can explain changes in the reaction orders for propane and hydrogen gas as a result of Sn alloying. Figure 4 shows that the

majority of the alloyed surfaces have a reaction order of 1 for propane, and that reaction orders for hydrogen gas predominantly vary from -1.0 to 0.5 for PtSn/Pt(100), Pt<sub>3</sub>Sn/Pt(111), and Pt<sub>2</sub>Sn/Pt(211) while the mean hydrogen reaction order is about 0, varying from -2.0 to 1.0, for Pt<sub>3</sub>Sn/Pt(100). Reaction orders of close to 1 for propane originate from a low hydrocarbon coverage on the surfaces due to the presence of Sn, as described in Table S20 of the Supporting Information. The negative and positive reaction orders for hydrogen originate from the uncertainty of the adsorption and transition state energies and corresponding changes in the reaction mechanism. Hydrogen can block sites leading to negative reaction orders, but surface hydrogen can also facilitate the removal of deep dehydrogenated surface species leading to positive reaction orders.

In comparison to the pure metal surfaces, all of the tin-doped surfaces except Pt<sub>3</sub>Sn/Pt(100) show lower activity compared to the pure metal surfaces as shown in Figure 5 and 6. This trend can be explained by the much higher reaction barriers observed for the PtSn/Pt(100), Pt<sub>3</sub>Sn/Pt(111), and Pt<sub>2</sub>Sn/Pt(211) surfaces when compared to the pure Pt(100), Pt(111), and Pt(211) surfaces, respectively (see also Table S5 and S6). Pt<sub>3</sub>Sn/Pt(100), however, displays a more diverse trend in the reaction barriers relative to Pt(100), as some of the barriers are equal or lower than the barriers on Pt(100), hence, the slightly higher activity observed for Pt<sub>3</sub>Sn/Pt(100) relative to Pt(100). Also, Pt<sub>3</sub>Sn/Pt(100) has generally the lowest reaction barriers among the four tin-doped surfaces, likely because of the open surface structure and low Sn to Pt ratio in the alloy. It is difficult to compare trends in the selectivity of the pure metal surfaces and the tin-doped surfaces as nearly flat distributions are observed for the pure and tin-doped surfaces for the (100) and (111) facets. The flat distribution speaks to a high degree of uncertainty in the selectivity based on the DFT functional. However, when analyzing the

selectivity to  $C_1$  and  $C_2$  products (Figure S5 and S6), it appears that Sn substitution does not change the selectivity significantly but that sites on the (100) facet are more likely responsible for undesirable C-C cleavage reactions relative to all other surface facets. If indeed the case, a high Sn coverage on the (100) facet could lead to a reduction in C-C cleavage selectivity due to a significantly reduced activity of this surface facet (even if the selectivity on the surface facet itself does not change significantly). In contrast, Pt(211) and Pt<sub>2</sub>Sn/Pt(211) both demonstrate a high selectivity to propylene; although Pt<sub>2</sub>Sn/Pt(211) has a tail extending to lower selectivity values (due to propyne production), hence, reducing the mean selectivity relative to Pt(211). However, the selectivity to  $C_1$  and  $C_2$  products (Figure S6) remains low independent of Sn doping. In general, while propylene desorption is favored on the tin-doped surfaces compared to the pure Pt surfaces, due to the weaker adsorption strength and increased reaction barriers as a result of the presence of tin, propane consumption and propylene production are reduced across all the doped surfaces except for Pt<sub>3</sub>Sn/Pt(100).

In this context, we also note that for Pt<sub>3</sub>Sn/Pt(100), the most important side products are methane and ethylene, while for PtSn/Pt(100), they are methane and acetylene, as seen in Table S21 of the Supporting Information. Acetylene becomes a dominant product on PtSn/Pt(100) due to a significantly reduced adsorption strength which permits its desorption. The reduced acetylene adsorption strength can again be explained by the high tin coverage and the lack of pure platinum bridge sites on PtSn/Pt(100). Ultimately, the production of triple bond species is, however, equilibrium limited at practical experimental conversions and hydrogen partial pressures (simulation results are performed at fixed pressure, i.e., zero conversion).

The predicted values for propylene selectivity, and other observable data, are dependent on the rate determining steps. Overall, early dehydrogenations steps are rate controlling on all the

surfaces. Figure 7 graphically describes the most important rate controlling steps. On Pt<sub>3</sub>Sn/Pt(100), both first dehydrogenation steps to the CH<sub>3</sub>CHCH<sub>3</sub>\* and CH<sub>3</sub>CH<sub>2</sub>CH<sub>2</sub>\* intermediates are partially rate controlling, with the pathway to CH<sub>3</sub>CHCH<sub>3</sub>\* having a higher average degree of rate control. Similar trends to Pt<sub>3</sub>Sn/Pt(100) are also seen on Pt<sub>3</sub>Sn/Pt(111) and Pt<sub>2</sub>Sn/Pt(211), however, both steps have more similar degrees of rate control and some degree of rate control is observed for the second dehydrogenation steps leading to the production of propylene, i.e., CH<sub>3</sub>CHCH<sub>3</sub> → CH<sub>3</sub>CHCH<sub>2</sub> + H and CH<sub>3</sub>CH<sub>2</sub>CH<sub>2</sub> → CH<sub>3</sub>CHCH<sub>2</sub> + H. In contrast, for PtSn/Pt(100), second dehydrogenation steps were found to be partially rate controlling alongside only the first dehydrogenation step to CH<sub>3</sub>CH<sub>2</sub>CH<sub>2</sub>\*.

Next, it is interesting to note that the identified rate determining steps based on propane consumption are similar to those observed based on the turnover frequency of propylene production, as described in the Supporting Information Figures S3 and S4. Initial, terminal dehydrogenation is somewhat less rate controlling for propylene production and initial, central dehydrogenation is somewhat more rate controlling. Again, for the PtSn/Pt(100) surface initial dehydrogenations are less rate controlling than secondary dehydrogenations and as expected, deep dehydrogenations to non-propylene products display no or a negative degree of rate control for propylene production.

## Calibration

In addition to the prior results discussed above, the models were also calibrated to the experimental selectivity and propylene turnover frequency, as previously discussed in the methods section. The experimental data can be viewed in the Supporting Information Table S8. Calibration informs the model by reducing the prior uncertainty derived from BEEF-vdW such

that the posterior simulations better explain the experimental data as compared with the prior simulations. This can be seen in Figures 8 and 9. The output of all of the turnover frequencies of the surfaces center around the reported turnover frequency. Selectivity to propylene for the calibrated models increases significantly, with all surfaces encapsulating the experimental data.

This calibration procedure not only affects the calibrated experimental quantities of interest, such as the TOF of propylene and selectivity to propylene, but also the reaction orders, apparent activation energies, and degrees of rate control for each surface. As seen in Figures 8 and 9, the differences between the calibrated and prior apparent activation energies and reaction orders are significant. The peaks of the apparent activation energy distributions center at approximately 1 eV, and the reaction orders in hydrogen gas are between -2 and 0. Calibration affects the degree of rate control of the reactions that are kinetically rate controlling, as seen in Figure 10. For Pt<sub>3</sub>Sn/Pt(100), Pt<sub>3</sub>Sn/Pt(111), and Pt<sub>2</sub>Sn/Pt(211), the kinetically rate controlling steps based on propane consumption remain the same, however,  $\text{CH}_3\text{CH}_2\text{CH}_3 \rightarrow \text{CH}_3\text{CHCH}_3 + \text{H}$  is now more clearly the dominant kinetic rate controlling step and other reactions are only partially rate controlling as shown by the high peaks close to zero. For PtSn/Pt(100), calibration results show that the first dehydrogenation reaction to  $\text{CH}_3\text{CH}_2\text{CH}_2^*$  and second dehydrogenation reactions to propylene from both  $\text{CH}_3\text{CH}_2\text{CH}_3^*$  and  $\text{CH}_3\text{CHCH}_3^*$  are all almost equally rate controlling contrary to the distribution in the non-calibrated model. Moreover, the reaction of  $\text{CH}_3\text{CH}_2\text{CH}_2 \rightarrow \text{CH}_3\text{CH}_2\text{CH} + \text{H}$ , found to be partially rate controlling in the uncalibrated model, is no longer observed to be rate controlling in the calibrated model. Experimental data can clearly not be explained with a partially rate controlling deep dehydrogenation step.

Next, the degree of kinetic rate control based on the turnover frequency of propylene is shown in Figure S7 of the Supporting Information. There is hardly any difference to the degree of rate control based on propane consumption. The only minor difference is observed for the PtSn/Pt(100) surface, where  $\text{CH}_3\text{CH}_2\text{CH}_3 \rightarrow \text{CH}_3\text{CHCH}_3 + \text{H}$  is now also found to be partially rate controlling. The similarity between the degree of rate control of propane consumption and propylene production is due to the generally high selectivity to propylene for all surfaces.

Finally, the evidence of the surfaces to describe the experimental kinetic observations can be compared using Bayes factors, as shown in Table 2, and then evaluated using Jeffreys' scale, in Table 3.<sup>56</sup> We find that there is hardly any evidence supporting any single Pt-Sn model as the active site for propane dehydrogenation to propylene. Given the general activity of all the Pt-Sn surface model considered, it is likely that all the surfaces participate in the dehydrogenation reaction. Although the Bayes factor indicates that the evidence supporting each of the surface models as the active site is hardly worthy mentioning, it is still interesting that the Bayes factor supporting Pt<sub>2</sub>Sn/Pt(211) as the active site over each of the other surfaces is highest. We previously also observed for the pure Pt surfaces that the step site has the highest likelihood of being the most relevant active site. In this context, Table S21 also shows that Pt<sub>2</sub>Sn/Pt(211) has the highest selectivity to propylene and other side products such as propyne, ethylene, ethyne, and methane are largely produced on the other Pt-Sn surface sites.

Studying the uncertainty within the functional energies and how they propagate through the microkinetic models helps generate a fuller understanding of the behavior of the chemistry on catalysts. Incorporating uncertainty allows for a more evidence-based understanding of reactions and helps create a fuller picture of the results. This can be seen in the comparisons of the microkinetic model results without incorporating uncertainty, as described in the Supporting

Information Table S12-S19. Major differences can be seen between the prior models of PtSn/Pt(100) and Pt<sub>2</sub>Sn/Pt(211). Bayesian models with functional uncertainty showed a higher average selectivity on Pt<sub>2</sub>Sn/Pt(211) compared to PtSn/Pt(100), while regular MKM models without functional uncertainty displays a higher selectivity to propylene for PtSn/Pt(100). This difference is due to small changes in the reaction energies and barriers leading to significant changes in the favorability of propylene desorption versus deeper dehydrogenation and undesirable side product formation on PtSn/Pt(100). These differences are critical for further understanding how reactions may proceed over Pt-Sn based catalysts. Calibration allows us to evaluate the model's fit to the data and directly shows us how informing on the data points impacts our models. It also allows for generation of evidence, allowing for direct comparisons of active site models which (with a sufficient number of experimental data at different reaction conditions) can help identify active sites and reaction mechanisms.

## Conclusions

To identify how platinum-tin alloys affect the propane dehydrogenation to propylene over Pt-Sn catalysts, multiple elementary reactions for the propane dehydrogenation were studied from first principles over four surface models: Pt<sub>3</sub>Sn/Pt(100), PtSn/Pt(100), Pt<sub>3</sub>Sn/Pt(111), and Pt<sub>2</sub>Sn/Pt(211). Mean-field microkinetic models were generated to give information that can directly be compared to experimental observation. Given the uncertainties in the DFT energies, we use the BEEF-vdW Model with Ensembles (BMwE) for generating the correlation structure of the DFT functional energy uncertainty for each surface model. In addition to testing at reported experimental conditions, we also calibrated our models to reported experimental data.

The prior, uncalibrated models, all show a high free site coverage, indicating a key impact of tin on all the platinum-tin surface alloys is reducing coke precursor production. In addition, the prior models showed that the addition of Sn leads to reduced activity across the tin-doped surfaces except for the low Sn coverage surface, Pt<sub>3</sub>Sn/Pt(100), where a slightly increased activity is likely. In other words, the activity modification due to the presence of Sn is surface facet dependent. Selectivity distributions for all the tin-doped surfaces are similar to their corresponding pure Pt surfaces. Unfortunately, the selectivity varies from 0 to 100% dependent on the functional for all but the stepped surfaces. Similar to the pure Pt(211) surface site, Pt<sub>2</sub>Sn/Pt(211) shows the highest selectivity to propylene amongst the Sn-doped surfaces. The stepped surfaces are also the only surface facets that are unable to display a high selectivity to C<sub>1</sub> and C<sub>2</sub> products. Based on the prior probability density, it is most likely that (100) surface facet sites are responsible for most observed C-C cleavage products, although C-C cleavage products can be produced on all active site models. We suggest that the experimentally observed higher selectivity in the presence of Sn is probably due to a reduced activity of a surface facet in the presence of Sn that promotes production of side products, e.g., large amounts of Sn reduce the activity of the (100) surface.

The rate controlling steps for propane consumption and propylene production across all surfaces are the first dehydrogenation steps of propane at the central and terminal carbon. Only for PtSn/Pt(100) do we observe that the initial dehydrogenation at the central carbon is not rate controlling. Instead, the second dehydrogenation steps are partially rate controlling for this surface.

The calibrated model showed all surfaces were highly selective to propylene production, and all the probability densities encapsulated the reported turnover frequencies and selectivities.

In addition, the rate controlling steps across the surfaces are similar to the uncalibrated models, with a somewhat higher probability of the initial C-H activation at the central carbon being most rate controlling. Again, the PtSn/Pt(100) surface is an exception to this observation since the initial dehydrogenation at the central carbon is not rate controlling on this surface and deep dehydrogenation steps remain most likely rate controlling for this surface. Through Bayesian inference and Jeffreys' scale, sites similar to the stepped Pt<sub>2</sub>Sn/Pt(211) have some evidence to be the active site in the experimental catalysts. However, the evidence is small and either more experimental data at different reaction conditions are needed or the computational uncertainties need to be significantly reduced to conclusively determine the active site for propane consumption and propylene production.

Though this study was comprehensive in studying surface alloys of different platinum facets, there is much debate over what are the most representative models of Pt-Sn alloys. Though models may include bulk alloys, in actuality, there are many possibilities, and we remain unsure how to describe the active site for these particular catalysts, especially when catalyst particle composition and distribution varies with catalyst synthesis, which may yield different alloys for catalyst particles, including the presence of pure metal surfaces as well. Finally, more kinetic experimental data, including additional TOFs, selectivities, reaction orders, apparent activation energies, and other reaction data are likely needed to further refine the calibration problem and perform a fuller model analysis.

## Supporting Information

Supporting information includes a supporting information portable document file (.pdf) with additional analysis and calculation results.

Optimized calculation geometries have been included as text (.txt) files.

## Acknowledgments

This work was supported by the Institute for Cooperative Upcycling of Plastics (iCOUP), an Energy Frontier Research Center funded by the U.S. Department of Energy (DOE), Office of Basic Energy Sciences under Contract DE-AC-02-07CH11358. In addition, initial partial support was provided by the National Science Foundation under grant number CBET-1534260. C.F. also acknowledges partial support from the National Science Foundation IGERT program under grant number 1250052. Computer resources were used from the National Energy Research Scientific Computing Center (NERSC) Contract No. DE-AC02-05CH11231, Pacific Northwest National Laboratory (Ringgold ID 130367, Grant Proposal 51711), and the University of South Carolina's High-Performance Computing Group.

## Figures and Tables

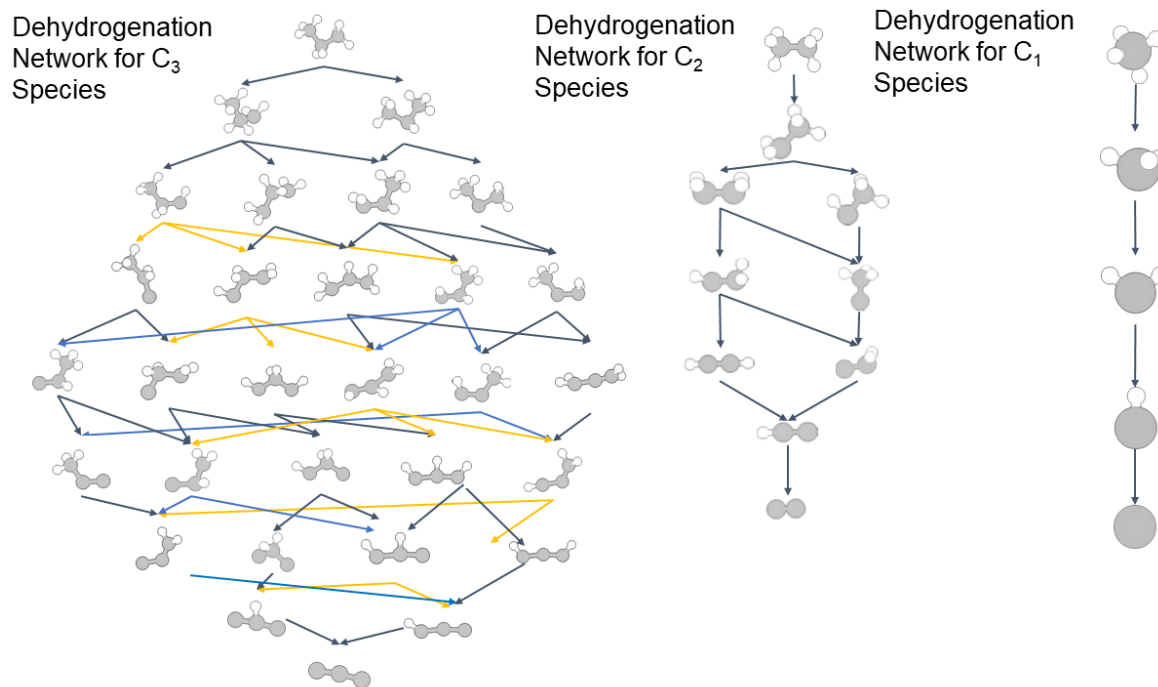


**Figure 1:** Dehydrogenation reaction network around C<sub>1-3</sub> species.

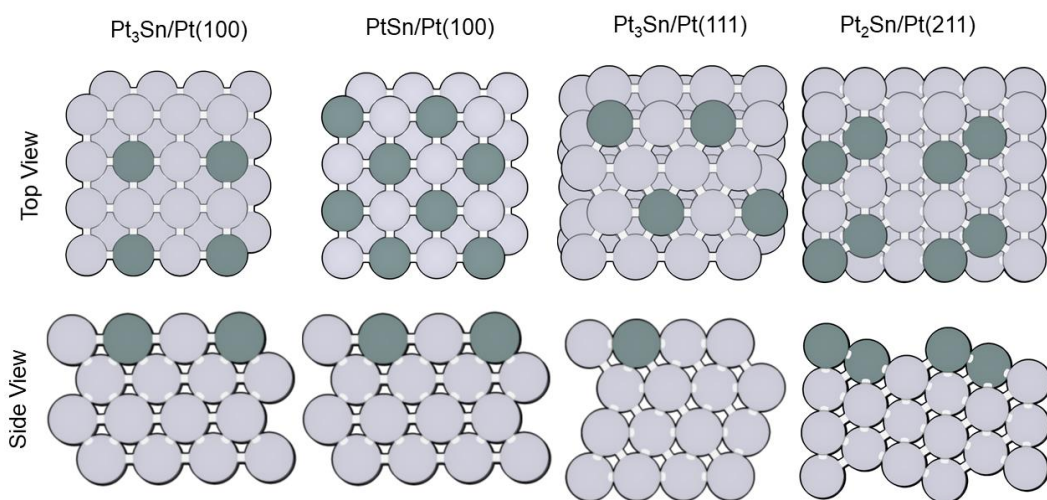


**Figure 2:** The four surfaces evaluated in this study.

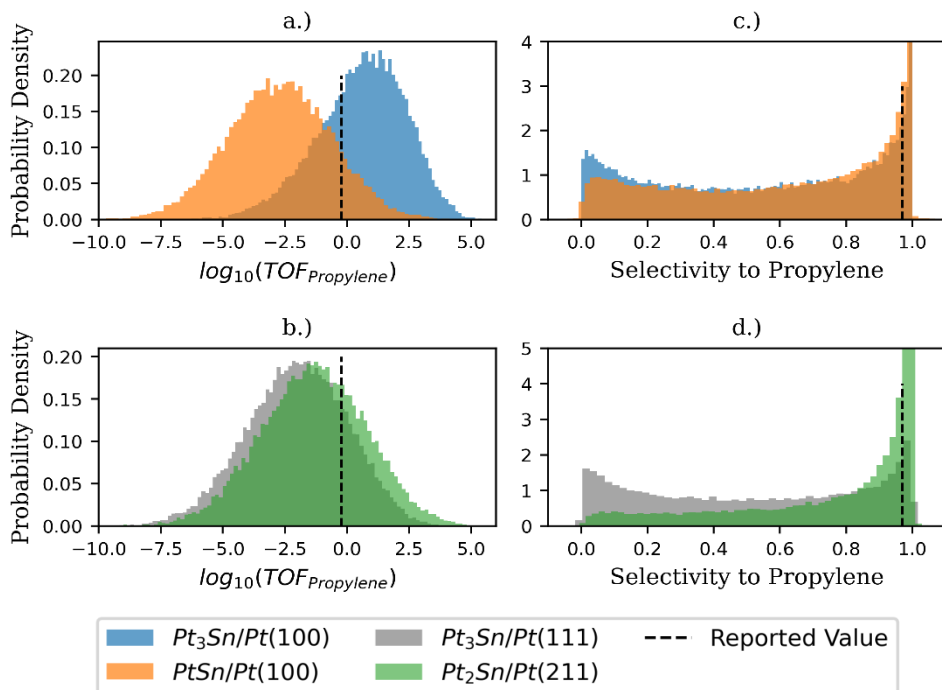


**Figure 3:** Histograms of the turnover frequency of propylene (TOF) and selectivity towards propylene on all four surfaces for the prior model, i.e., no calibration.

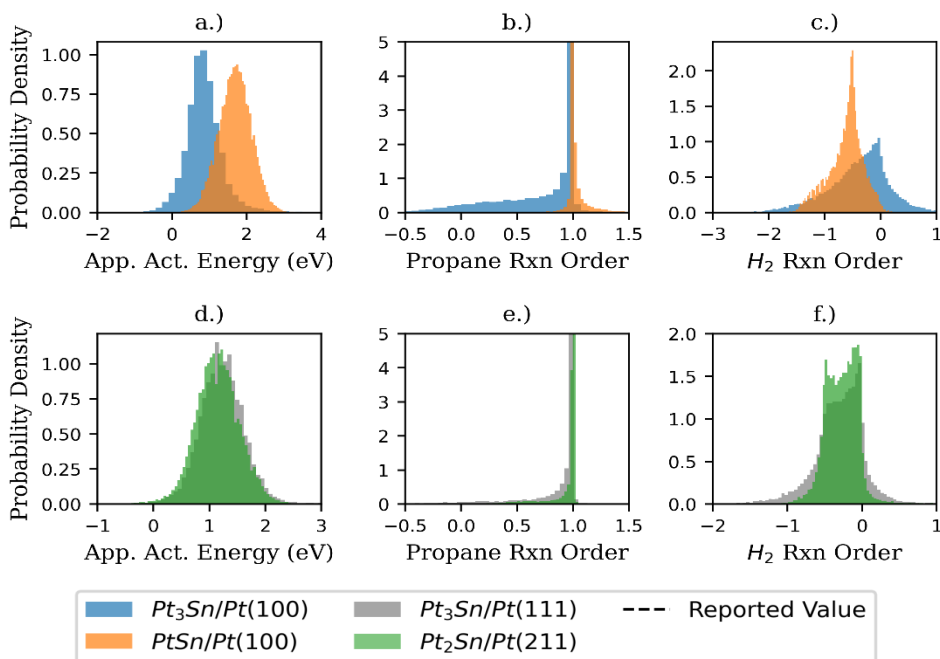


**Figure 4:** Apparent activation energy, reaction order of propane, and reaction order of H<sub>2</sub> for all four surfaces calculated using the TOF of propylene for the prior model, i.e., no calibration.

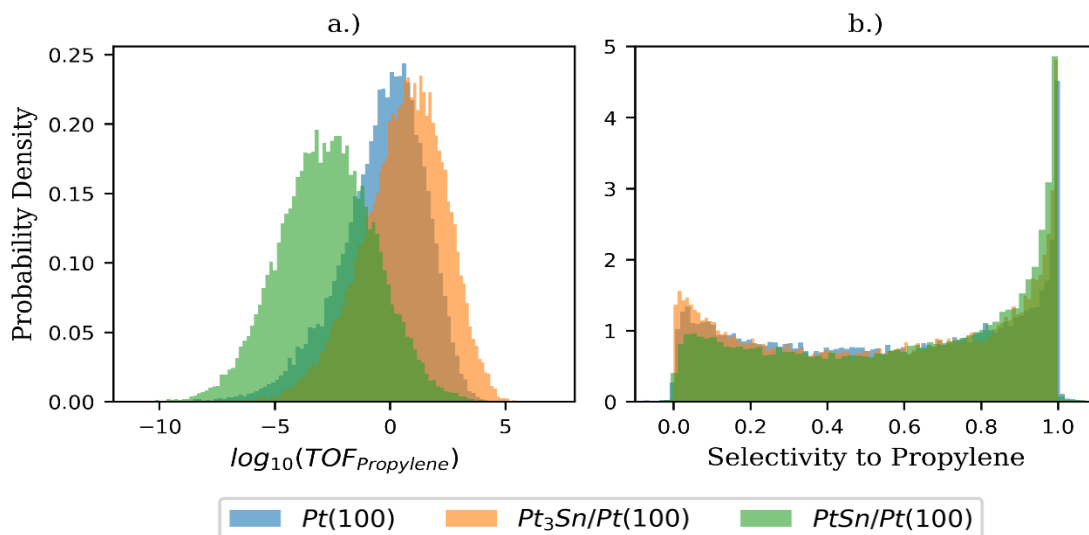


**Figure 5:** Comparison between pure Pt(100) surface as modeled in this work and in Fricke et al.<sup>29</sup> and its corresponding tin-doped surfaces prior models studied in this work.

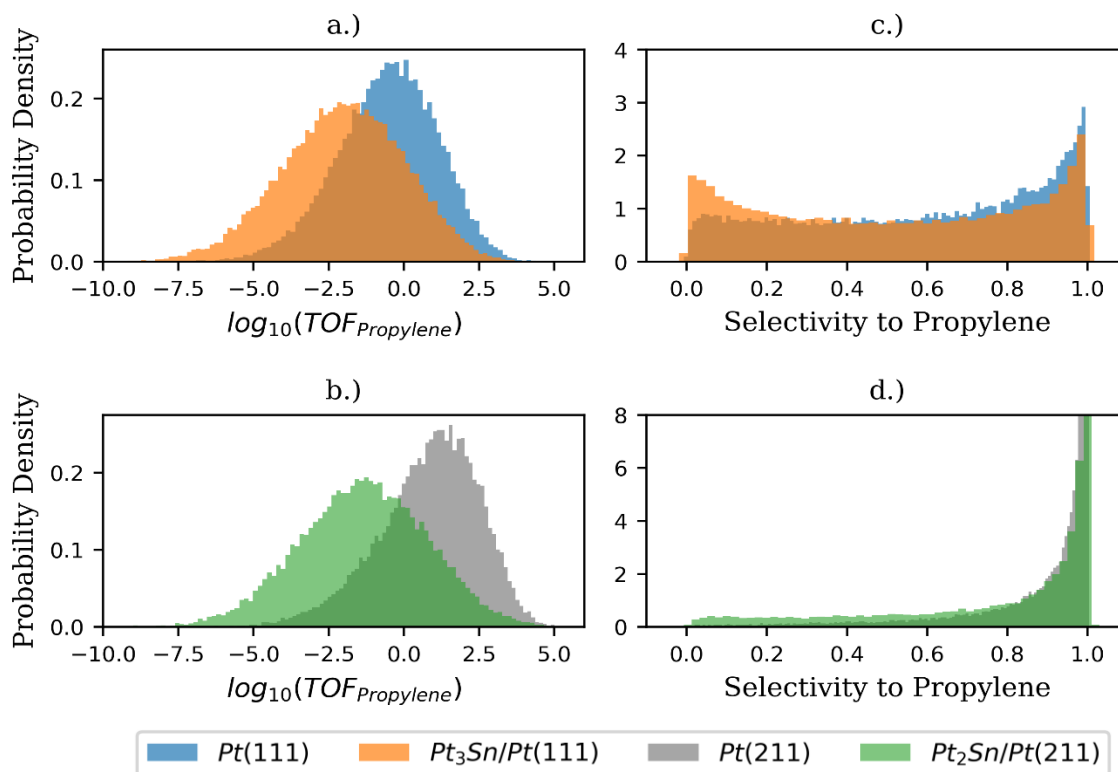


**Figure 6:** Comparison between pure Pt(111) and Pt(211) surfaces as modeled in this work and in Fricke et al.<sup>29</sup> versus their corresponding tin-doped surface prior models studied in this work.

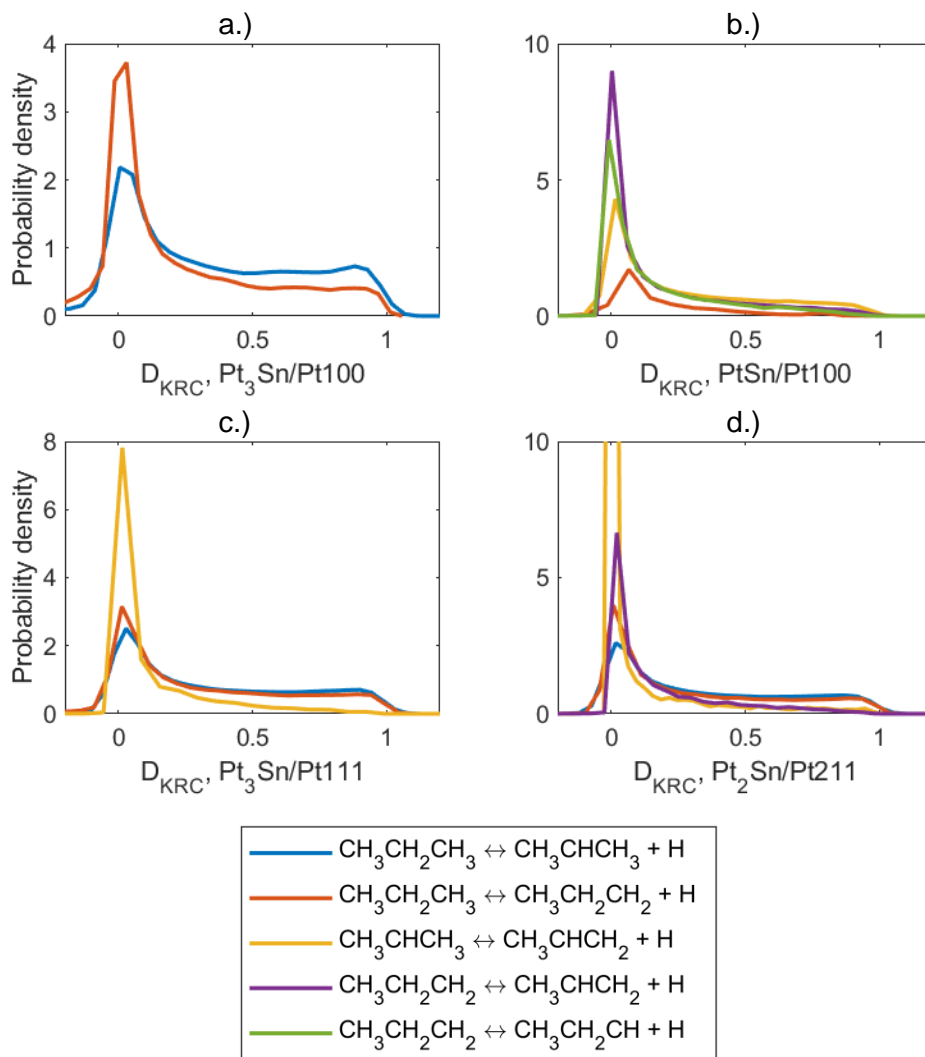


**Figure 7:** Degree of kinetic rate control ( $D_{KRC}$ ) for the most important steps on all four Pt-Sn alloy surfaces calculated using the TOF of propane consumption. (a)  $\text{Pt}_3\text{Sn/Pt}(100)$ , (b)  $\text{PtSn/Pt}(100)$ , (c)  $\text{Pt}_3\text{Sn/Pt}(111)$ , (d)  $\text{Pt}_2\text{Sn/Pt}(211)$ .

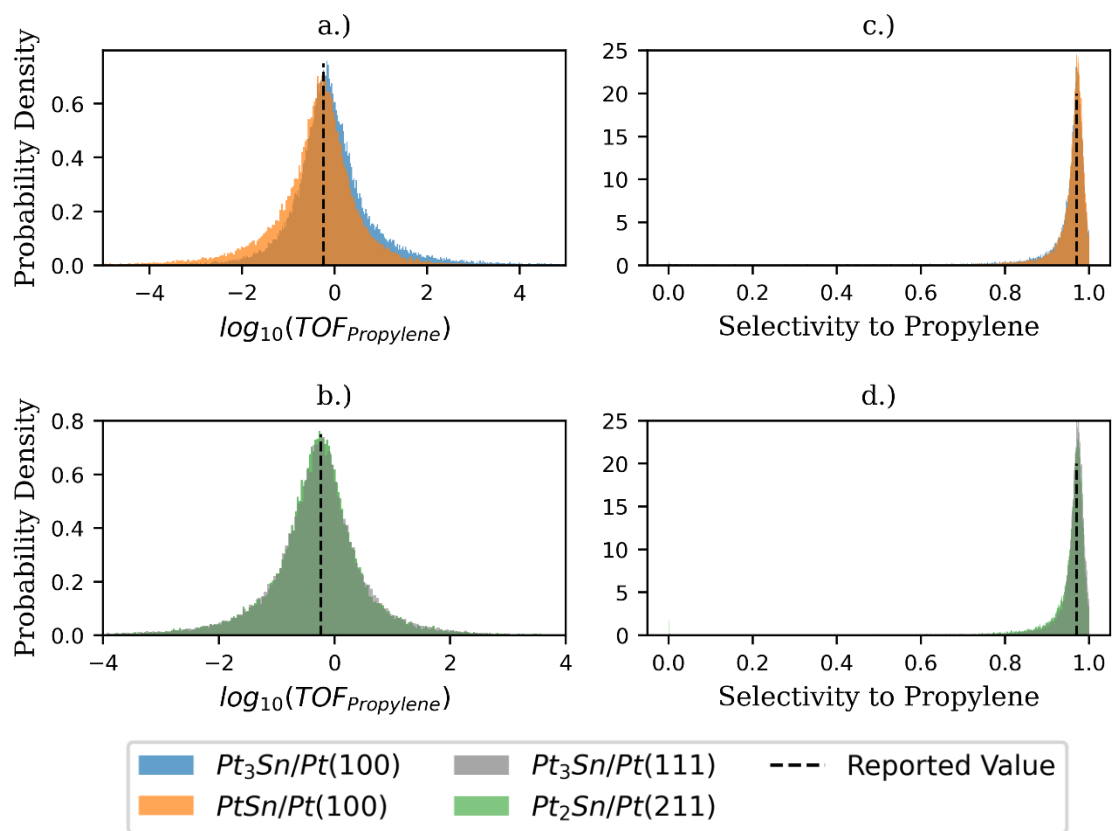


**Figure 8:** Calibrated models for TOFs of propylene production and selectivity towards propylene on all four Pt-Sn surface models.

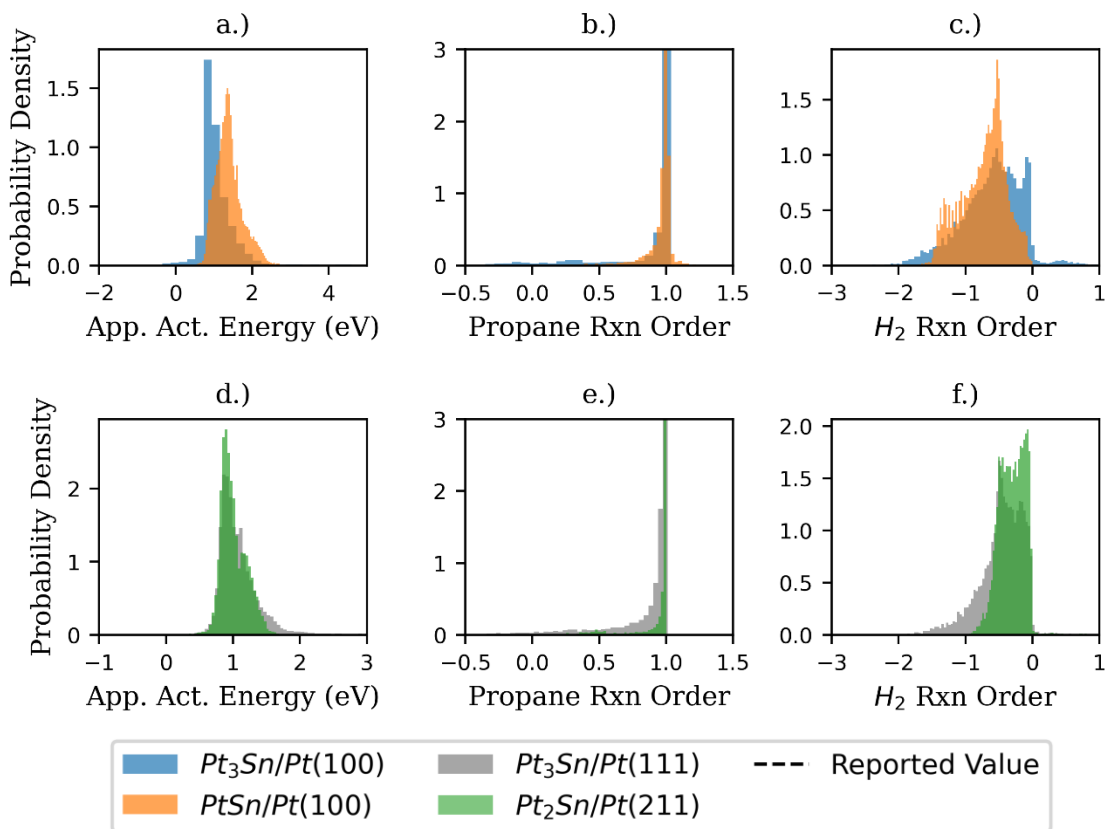


**Figure 9:** Calibrated models for apparent activation energies and reaction orders for propylene production for all four Pt-Sn alloy surface models.

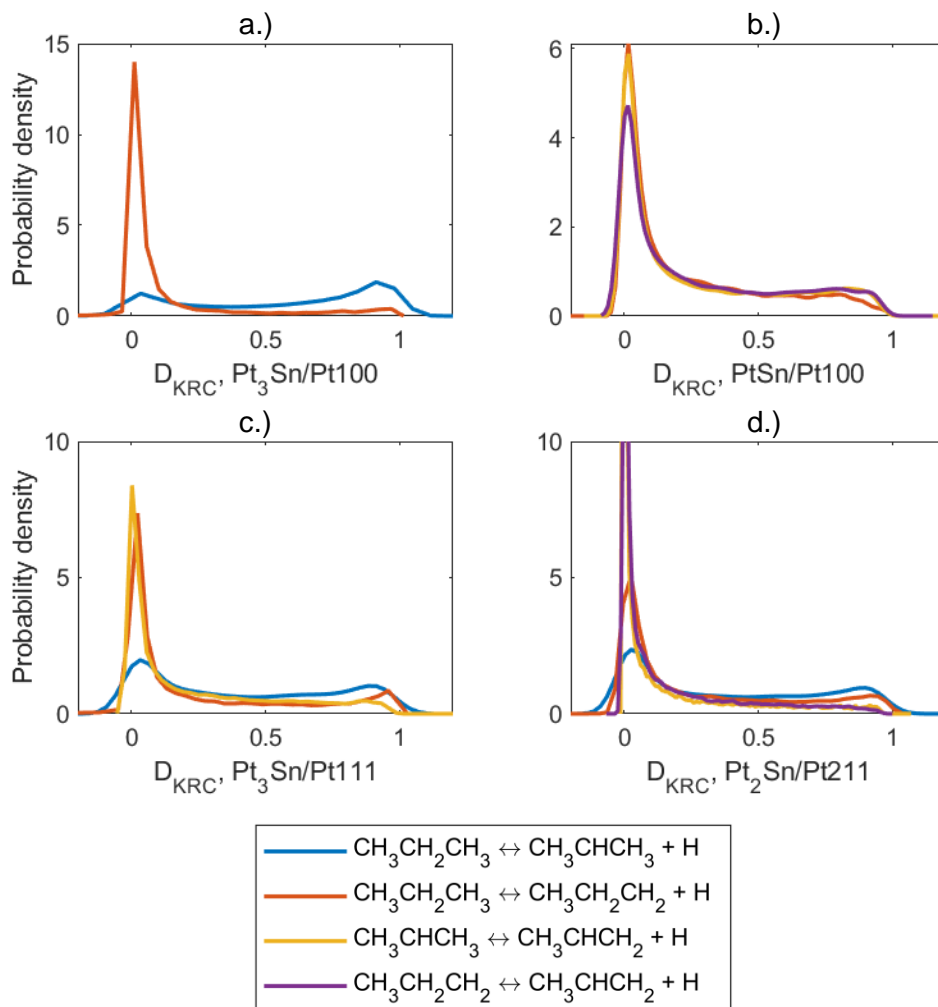


**Figure 10:** Degree of kinetic rate control ( $D_{KRC}$ ) for the most important steps on all four Pt-Sn alloy surfaces calculated using the TOF of propane consumption calibrated to the experimental data.<sup>6</sup>

**Table 1:** Activation free energy barriers of select reactions that occur early in the dehydrogenation mechanism. Energies referenced to gaseous methane and hydrogen at 1 bar and 792K. All reactions occur on the surface.

Chemical Reaction	Reaction Number	Free Energy of the Transition State, (eV)			
		Pt <sub>3</sub> Sn/ Pt(100)	PtSn/ Pt(100)	Pt <sub>3</sub> Sn/ Pt(111)	Pt <sub>2</sub> Sn/ Pt(211)
CH <sub>3</sub> CH <sub>2</sub> CH <sub>3</sub> → CH <sub>3</sub> CHCH <sub>3</sub> +H	1	0.92	1.33	1.48	1.35
CH <sub>3</sub> CH <sub>2</sub> CH <sub>3</sub> → CH <sub>3</sub> CH <sub>2</sub> CH <sub>2</sub> +H	2	1.01	1.34	1.59	1.30
CH <sub>3</sub> CHCH <sub>3</sub> → CH <sub>3</sub> CHCH <sub>2</sub> +H	3	0.90	1.39	1.12	0.97
CH <sub>3</sub> CH <sub>2</sub> CH <sub>2</sub> → CH <sub>3</sub> CHCH <sub>2</sub> +H	4	0.87	1.41	1.05	1.13
CH <sub>3</sub> CH <sub>2</sub> CH <sub>3</sub> → CH <sub>3</sub> +CH <sub>2</sub> CH <sub>3</sub>	5	2.62	2.18	3.08	2.58
CH <sub>3</sub> CHCH <sub>3</sub> → CH <sub>3</sub> CH+CH <sub>3</sub>	6	1.89	2.36	2.09	2.25
CH <sub>3</sub> CHCH <sub>3</sub> → CH <sub>3</sub> CCH <sub>3</sub> +H	7	0.67	1.56	1.09	1.24
CH <sub>3</sub> CH <sub>2</sub> CH <sub>2</sub> → CH <sub>3</sub> CH <sub>2</sub> +CH <sub>2</sub>	8	1.69	2.39	2.01	2.14
CH <sub>3</sub> CH <sub>2</sub> CH <sub>2</sub> → CH <sub>3</sub> +CH <sub>2</sub> CH <sub>2</sub>	9	2.38	2.68	2.71	2.71
CH <sub>3</sub> CH <sub>2</sub> CH <sub>2</sub> → CH <sub>2</sub> CH <sub>2</sub> CH <sub>2</sub> +H	10	1.03	1.39	1.32	1.31
CH <sub>3</sub> CH <sub>2</sub> CH <sub>2</sub> → CH <sub>3</sub> CH <sub>2</sub> CH +H	11	0.74	1.37	1.02	1.15
CH <sub>3</sub> CH <sub>2</sub> CH → CH <sub>3</sub> CH <sub>2</sub> C +H	14	0.64	1.70	0.58	0.99
CH <sub>3</sub> CH <sub>2</sub> CH → CH <sub>3</sub> CHCH+H	15	0.86	0.59	0.94	1.00
CH <sub>3</sub> CH <sub>2</sub> CH → CH <sub>2</sub> CH <sub>2</sub> CH+H	16	1.17	1.28	1.38	1.68
CH <sub>3</sub> CHCH <sub>2</sub> → CH <sub>3</sub> +CHCH <sub>2</sub>	20	1.53	3.00	2.10	2.06
CH <sub>3</sub> CHCH <sub>2</sub> → CH <sub>3</sub> CH+CH <sub>2</sub>	21	1.94	2.51	2.16	2.28
CH <sub>3</sub> CHCH <sub>2</sub> → CH <sub>3</sub> CCH <sub>2</sub> +H	22	0.78	1.72	1.09	1.62
CH <sub>3</sub> CHCH <sub>2</sub> → CH <sub>3</sub> CHCH+H	23	0.85	1.11	1.09	1.58
CH <sub>3</sub> CHCH <sub>2</sub> → CH <sub>2</sub> CHCH <sub>2</sub> +H	24	0.89	0.79	1.22	1.29
CH <sub>2</sub> CHCH <sub>2</sub> → CH <sub>2</sub> CCH <sub>2</sub> +H	38	2.32	2.15	1.09	1.58
CH <sub>3</sub> CHCH → CH <sub>3</sub> +CHCH	39	1.53	2.89	1.77	1.81
CH <sub>3</sub> CHCH → CH <sub>3</sub> CH+CH	40	2.05	3.49	1.80	2.95
CH <sub>3</sub> CHCH → CH <sub>3</sub> CHC+H	41	0.92	1.49	0.61	0.64
CH <sub>3</sub> CHCH → CH <sub>3</sub> CCH+H	42	1.25	2.15	0.90	0.75
CH <sub>3</sub> CHCH → CH <sub>2</sub> CHCH+H	43	1.36	1.87	1.25	0.99

$\text{CH}_3\text{CCH}_2 \rightarrow \text{CH}_3+\text{CH}_2\text{C}$	44	1.52	2.79	1.57	1.75
$\text{CH}_3\text{CCH}_2 \rightarrow \text{CH}_3\text{C}+\text{CH}_2$	45	0.99	3.00	1.87	2.40
$\text{CH}_3\text{CCH}_2 \rightarrow \text{CH}_2\text{CCH}_2+\text{H}$	46	1.00	1.55	1.17	1.62
$\text{CH}_3\text{CCH}_2 \rightarrow \text{CH}_3\text{CCH}+\text{H}$	47	0.95	2.15	0.88	0.62

**Table 2:** Evidence and Bayes factor for each Pt-Sn surface as compared to the other Pt-Sn surfaces.

Surface	Evidence	Bayes factor relative to			
		Pt <sub>3</sub> Sn/Pt100	PtSn/Pt100	Pt <sub>3</sub> Sn/Pt111	Pt <sub>2</sub> Sn/Pt211
<b>Pt<sub>3</sub>Sn/Pt100</b>	$3.57 \times 10^{-3}$	1.00	0.86	0.85	0.41
<b>PtSn/Pt100</b>	$4.13 \times 10^{-3}$	1.16	1.00	0.98	0.47
<b>Pt<sub>3</sub>Sn/Pt111</b>	$4.20 \times 10^{-3}$	1.18	1.02	1.00	0.48
<b>Pt<sub>2</sub>Sn/Pt211</b>	$8.71 \times 10^{-3}$	2.44	2.11	2.08	1.00

**Table 3:** Jefferys' scale for Bayes factors,  $B_{12} = p(D|M_1)/p(D|M_2)$ <sup>56</sup>

$B_{12}$	Evidence for $M_1$
1 - 3.2	Not worth more than a bare mention
3.2 - 10	Positive
10 - 100	Strong
> 100	Very strong

## References

1. Sattler, J. J. H.; Ruiz-Martinez, J; Santillan-Jimenez, E.; Weckhuysen, B.M. Catalytic Dehydrogenation of Light Alkanes on Metals and Metal Oxides. *Chem. Rev.*, **2014**, *114*, 10613-10653
2. Wang, Y.; Hu, P.; Yang, J.; Zhu, Y.; Chen, D.; C–H bond activation in light alkanes: a theoretical perspective, *Chem. Soc. Rev.*, **2021**, *50*, 4299-4358
3. Zhao, Z.; Jiang, J.; Wang, F. An economic analysis of twenty light olefin production pathways. *Journal of Energy Chemistry*, **2021**, *56*, 193-202
4. Wang, J.; Chang, X.; Chen, S.; Sun, G.; Zhou, X.; Vovk, E.; Yang, Y.; Deng, W; Zhao, Z; Mu, R.; Pei, C.; Gong, J.; On the Role of Sn Segregation of Pt-Sn Catalysts for Propane Dehydrogenation. *ACS Catal.*, **2021** , *11* (8), 4401-4410
5. Zhua, H; Anjum, D. H; Wang, Q.; Abou-Hamad, E.; Emsley, L.; Dong , H.; Laveille, P.; Li, L.; Samal, A. K.; Basset, J.; Sn surface-enriched Pt–Sn bimetallic nanoparticles as a selective and stable catalyst for propane dehydrogenation, *J. Catal.*, **2014**, *320*, 52-62
6. Bari as, O. A.; Holmen, A.; Blekkan, E. A. Propane Dehydrogenation over Supported Pt and Pt–Sn Catalysts: Catalyst Preparation, Characterization, and Activity Measurements. *J. Catal.*, **1996**, *158*, 1–12.
7. Kaylor, N.; Davis, R. J.; Propane dehydrogenation over supported Pt-Sn nanoparticles, *J. Catal.*, **2018**, *367*, 181-193
8. A. Iglesias-Juez, A. M. Beale, K. Maaijen, T. C. Weng, P. Glatzel, B. M. Weckhuysen, A combined in situ time-resolved UV-Vis, Raman and high-energy resolution X-ray absorption spectroscopy study on the deactivation behavior of Pt and PtSn propane dehydrogenation catalysts under industrial reaction conditions. *J. Catal.*, **2010**, *276*, 268–279.
9. Xiong, H.; Lin, S.; Goetze, J.; Pletcher, P.; Guo, H.; Kovarik, L.; Artyushkova, K.; Weckhuysen, B. M; Datye, A. K.; Thermally Stable and Regenerable Platinum–Tin Clusters for Propane Dehydrogenation Prepared by Atom Trapping on Ceria, *Angew.Chem.Int. Ed.*, **2017**, *56*, 8986 –899
10. Motagamwala, A.H.; Almallahi, R.; Wortman, J.; Igenegbai, V. O.; Linic, S.; Stable and selective catalysts for propane dehydrogenation operating at thermodynamic limit, *Science* ,**2021**, *373* (6551), 217-222
11. Hannagan, R. T.; Giannakakis, G.; Reocreux, R.; Schumann, J.; Finzel, J.; Wang, Y.; Michaelides, A.; Deshlarhra, P.; Christopher, P.; Flytzani-Stephanopoulos, M.; Stamatakis,

- M.; Sykes, E. C. H.; First-principles design of a single-atom–alloy propane dehydrogenation catalyst, *Science*, **2021**, 372 (6549), 1444-1447
12. Shi, L.; Deng, G. M.; Li, W. C.; Miao, S.; Wang, Q. N.; Zhang, W. P.; Lu, A. H. Al<sub>2</sub>O<sub>3</sub> nanosheets rich in pentacoordinate Al<sup>3+</sup> ions stabilize Pt-Sn clusters for propane dehydrogenation. *Angew. Chem., Int. Ed.*, **2015**, 54, 13994–13998.
  13. Xu, Z.; Yue, X.; Bao, X.; Xie, Z.; Zhu, H. Propane Dehydrogenation over Pt Clusters Localized at the Sn Single-Site in Zeolite Framework, *ACS Catal.* **2020**, 10, 1, 818–828.
  14. Iglesias-Juez, A.; Beale, A. M.; Maaijen, K.; Weng, T.C.; Glatzel, P.; Weckhuysen, B.M.; A combined in situ time-resolved UV–Vis, Raman and high-energy resolution X-ray absorption spectroscopy study on the deactivation behavior of Pt and Pt single bond Sn propane dehydrogenation catalysts under industrial reaction conditions. *J. Catal.*, **2010**, 276 (2), 268-279
  15. Pham, H. N.; Sattler, J. H. B; Weckhuysen, B. M.; Datye, A. K; *ACS Catal.*, **2016**, 6, 4, 2257–2264
  16. Deng, L; Shishido, T.; Teramura, K.; Tanaka, T. Effect of reduction method on the activity of Pt–Sn/SiO<sub>2</sub> for dehydrogenation of propane. *Catalysis Today*, **2014**, 232, 33-39
  17. Zhang, Y.; Zhou, Y.; Qiu, A.; Wang, Y.; Xu, Y. Wu, P. Propane dehydrogenation on PtSn/ZSM-5 catalyst: Effect of tin as a promoter. *Catal. Comm.*, **2006**, 7 (11), 860-866
  18. Duan, Y.; Zhou, Y.; Zhang, Y.; Sheng, X.; Xue, M. Effect of Sodium Addition to PtSn/AlSBA-15 on the Catalytic Properties in Propane Dehydrogenation, *Catalysis Letters*, **2011**, 141, 120-127.
  19. Larsson, M.; Andersson, B.; Barias, O.A., Holmen, A.; The use of the H<sub>2</sub>-D<sub>2</sub> equilibration reaction as a probe reaction to study the deactivation on Pt/Al<sub>2</sub>O<sub>3</sub> and Pt-Sn/Al<sub>2</sub>O<sub>3</sub> catalysts during propane dehydrogenation, *Studies in Surface Science and Catalysis*, **1994**, 88, 233-240
  20. Wu, J.; Sharada, S. M.; Ho. C.; Hauser, A. W.; Head-Gordon, M. Ethane and propane dehydrogenation over PtIr/Mg(Al)O. *Appl. Catal. A*, **2015**, 506, 25-32
  21. Barias, O.A.; Holmen, A.; Blekkan, E.A, Propane dehydrogenation over supported platinum catalysts: effect of tin as a promoter. *Catalysis Today*, **1995**, 24 (3), 361-364

22. Deng, L. Miura, K. Shishido, T.; Hosokawa, S.; Teramura, K.; Tanaka, T. Dehydrogenation of Propane over Silica-Supported Platinum–Tin Catalysts Prepared by Direct Reduction: Effects of Tin/Platinum Ratio and Reduction Temperature, *ChemCatChem*, **2014**, 6, 2680 – 2691
23. Nam, J.; Celik, F.; Effect of Tin in the Bulk of Platinum–Tin Alloys for Ethane Dehydrogenation. *Topics in Catalysis*, **2020**, 63, 700–713
24. Yang, M.; Zhu, Y.; Zhou, X.; Chen, D. First-Principles Calculations of Propane Dehydrogenation over PtSn Catalysts, *ACS Catal.* **2012**, 2, 6, 1247–1258
25. Nykanen, L.; Honkala, K. Density Functional Theory Study on Propane and Propene Adsorption on Pt(111) and PtSn Alloy Surfaces. *J. Phys. Chem. C* , **2011**, 115 (19), 9578–9586.
26. Honkala, Nykanen, Selectivity in Propene Dehydrogenation on Pt and Pt<sub>3</sub>Sn Surfaces from First Principles *ACS Catal.* **2013**, 3, 12, 3026–3030
27. Hook, A. Massa, J. D.; Celik, F. E. Effect of Tin Coverage on Selectivity for Ethane Dehydrogenation over Platinum-Tin Alloys. *J. Phys. Chem. C* 2016, 120, 48, 27307–27318
28. Wang, T.; Abild-Pedersen, F.; Identifying factors controlling the selective ethane dehydrogenation on Pt-based catalysts from DFT based micro-kinetic modeling. *Journal of Energy Chemistry*, **2021**, 37-40
29. Fricke, C; Rajbanshi, B.; Walker, E. A.; Terejanu, G.; Heyden, A.; Propane Dehydrogenation on Platinum Catalysts: Identifying the Active Sites through Bayesian Analysis, *ACS Catal.*, **2022**, 12, 2487-2498
30. Kresse, G.; Furthmüller, J., Efficiency of ab-initio total energy calculations for metals and semiconductors using a plane-wave basis set. *Comput. Mat. Sci.*, **1996**, 6 (1), 15-50
31. Kresse, G.; Furthmüller, J. Efficient iterative schemes for ab initio total-energy calculations using a plane-wave basis set. *Phys. Rev. B*, **1996**, 54 (16), 11169
32. Kresse, G.; Hafner, J. Ab initio molecular dynamics for liquid metals. *Phys. Rev. B*, **1993**, 47 (1), 558
33. Wellendorff, J; Lundgaard, K.T; Møgelhøj, A.; Petzold, V.; Landis, D.D.; Nørskov, J.K; Bligaard, T.; Jacobsen, K.W. Density functionals for surface science: Exchange-correlation model development with Bayesian error estimation. *Phys. Rev. B*, **2012**, 85, 235149

34. Blochl, P.E. “Projector augmented-wave method”, *Phys. Rev. B*, 1994, 50,17953
35. Kresse, G.; Halfer, J. “Norm-conserving and ultrasoft pseudopotentials for first-row and transition elements” *J. Phys. Condens. Matter*, **1994**, 6,8245
36. Monkhorst, H.; Pack, J. Special points for Brillouin-zone integrations. *Phys. Rev. B*, **1976**, 13, 5188
37. Pack, J.; Monkhorst, H. Special points for Brillouin-zone integrations. *Phys. Rev. B*, **1977**, 16, 1748
38. Haworth, N. L.; Wang, Q.; Coote, M. L., “Modeling Flexible Molecules in Solution: A pKa Case Study.” *J. Phys. Chem. A.*, **2017**, 121 (27), 5217-5225.
39. Henkelman, G.; Jónsson, H. A climbing image nudged elastic band method for finding saddle points and minimum energy paths. *J. Chem. Phys.*, **2000**, 113, 9901-9904
40. Henkelman, G.; Jónsson, H. Improved tangent estimate in the nudged elastic band method for finding minimum energy paths and saddle points. *J. Chem. Phys.*, **2000**, 113, 9978-9985
41. Henkelman, G.; Jónsson, H. A dimer method for finding saddle points on high dimensional potential surfaces using only first derivatives. *J. Chem. Phys.*, **1999**, 111, 7010
42. Heyden, A. ; Bell, A. T.; Keil, F. J. Efficient methods for finding transition states in chemical reactions: Comparison of improved dimer method and partitioned rational function optimization method. *J. Chem. Phys.*, **2005**, 123, 224101
43. Medford, A. J.; Wellendorf, J.; Vojvodic, A.; Studt, F.; Abild-Pedersen, F.; Jacobsen, K.; Bligaard, T.; Norskov, J.; Assessing the reliability of calculated catalytic ammonia synthesis rates. *Science*, **2014**, 345 (6193), 197-200
44. Walker E. A.,; Mitchell, D.; Terejanu, G. A.; Heyden, A. Identifying Active Sites of the Water–Gas Shift Reaction over Titania Supported Platinum Catalysts under Uncertainty” *ACS Catal.*, **2018**, 8, 3990-3998
45. Walker, E.; Ammal, S. C.; Terejanu, G. A.; Heyden, A. Uncertainty Quantification Framework Applied to the Water–Gas Shift Reaction over Pt-Based Catalysts. *J. Phys. Chem. C.*, **2016**, 120, 10328– 10339
46. Cramer, J. S. *Logit Models from Economics and Other Fields*; Cambridge University Press: Cambridge, **2003**; pp 149–157.

47. Prudencio E.E., Schulz K.W. (2012) The Parallel C++ Statistical Library ‘QUESO’: Quantification of Uncertainty for Estimation, Simulation and Optimization. In: *Alexander M. et al. (eds) Euro-Par 2011: Parallel Processing Workshops. Euro-Par 2011. Lecture Notes in Computer Science*, Bordeaux, France, August 29 – September 2, 2011. Springer, Berlin, Heidelberg, **2011**, vol 7155. pp 398-407
48. Horvatits, C.; Lee, J.; Kyriakidou, E.A; Walker, E.A. Characterizing Adsorption Sites on Ag/SSZ-13 Zeolites: Experimental Observations and Bayesian Inference. *J. Phys. Chem. C*, **2020**, *124* (35), 19174-19186
49. Walker, E..A.; Ravisankar, K.; and Savara, A; CheKiPEUQ Intro 2: Harnessing Uncertainties from Data Sets, Bayesian Design of Experiments in Chemical Kinetics. *ChemCatChem.*, **2020**,*12*, 5401-5410.
50. Collinge, G.; Yuk, S. F.; Nguyen, M.; Lee, M.; Glezakou, V.; Rousseau. Effect of Collective Dynamics and Anharmonicity on Entropy in Heterogenous Catalysis: Building the Case for Advanced Molecular Simulations. *ACS Catal.*, **2020**, *10* , 9236-9260
51. Sprowl, L.H.; Campbell, C. T.; Arnadottir, L.; Hindered Translator and Hindered Rotor Models for Adsorbates: Partition Functions and Entropies. *J. Phys. Chem. C*, **2016**, *120*, 18, 9719-9731
52. Jorgensen, M.; Gronbeck, H.; Adsorbate Entropies with Complete Potential Energy Sampling in Microkinetic Modeling. *J. Phys. Chem C*, **2017**, *121*, 13, 7199-7207
53. Campbell, C. T. Future Directions and Industrial Perspectives Micro-and Macro-Kinetics: Their Relationship in Heterogeneous Catalysis. *Top. Catal.*, **1994**, *1*, 353– 366
54. Campbell, C. T. The Degree of Rate Control: A Powerful Tool for Catalysis Research. *ACS Catal.* **2017**, *7*, 2770–2779
55. Campbell, C. T. Finding the Rate-Determining Step in a Mechanism: Comparing DeDonder Relations with the “Degree of Rate Control”. *J. Catal.*, **2001**, *204*, 520– 524
56. Jeffreys, H., *The Theory of Probability*; Oxford University Press:Oxford, **1939**.

For Table of Contents Only

